# Supplemental Figures and Figure legends for:

## An MHC-I- and galectin-9-dependent trap formed by cancer-associated fibroblasts restricts the anti-tumor function of CD8+ T cells

# Supplementary Figure S1

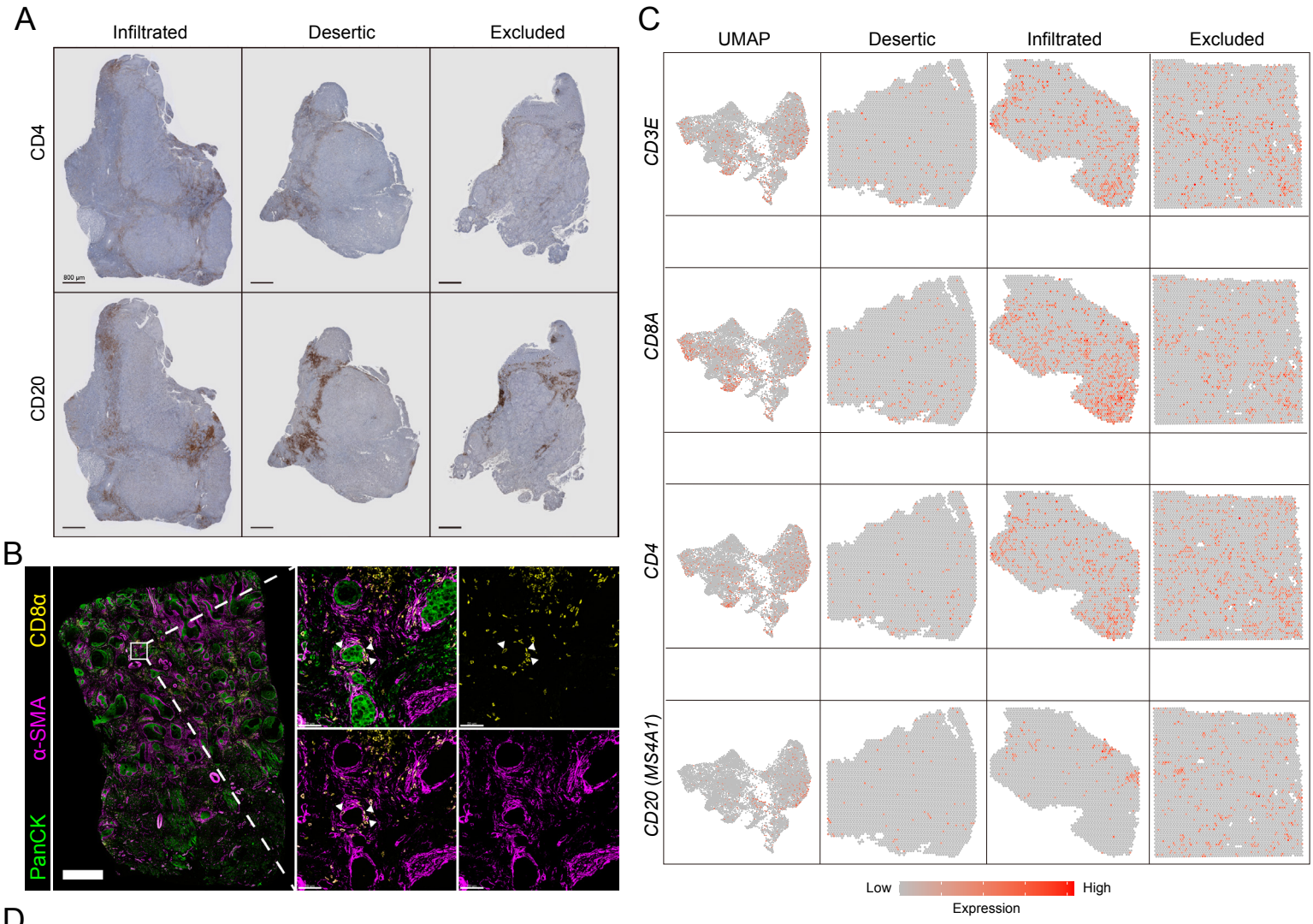

**Supplementary Figure S1.**

Heterogeneity of spatial cell distribution and gene expression patterns among three immune types of HNSCC. **A,** IHC staining of CD4 and CD20 of the infiltrated, desertic and excluded immune type of HNSCC. **B,** Large scale of multiplex immunofluorescence of PanCK (green), CD8α (yellow), α-SMA (wine) of the excluded immune type of HNSCC. The representative region was labelled with white rectangle and magified. **C,** Expression distribution of lymphocyte-associated genes (*CD3E*, *CD8A*, *CD4* and *MS4A1*) in the specimens of spatial transcriptome analysis. **D,** The expression and distribution of top 5 markers of cluster 9, including *COL11A1*, *GRP*, *HOXB2*, *BMP8A*, *NKD1* and *ST6GAL2*. **E,** The expression and distribution of *COL11A1, COL11A2* and *COL12A1* in the three specimens.

Supplementary Figure S2

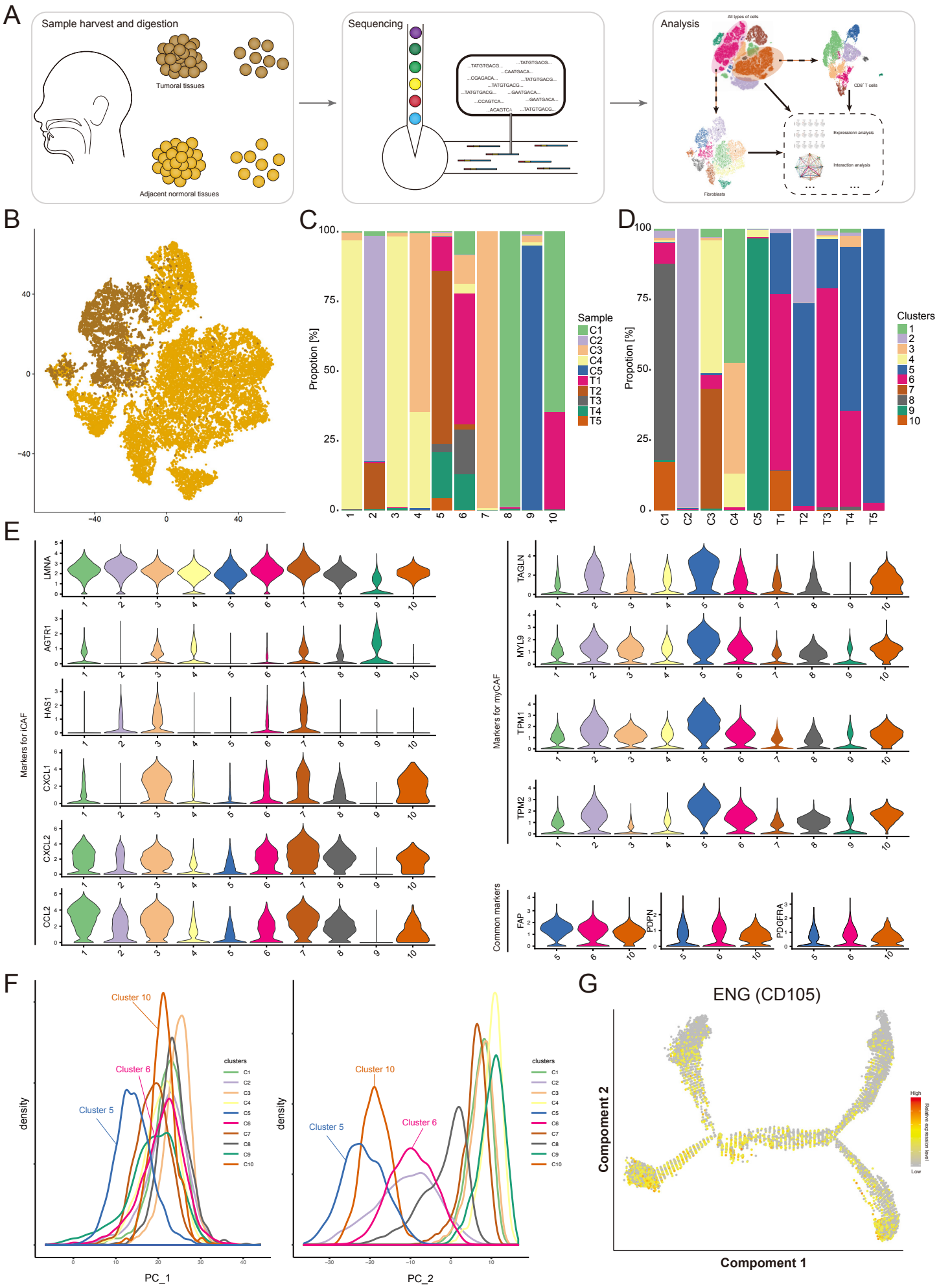

**Supplementary Figure S2.**

Single-cell RNA sequencing results of fibroblasts from normal and tumoral tissues of HNSCC. **A,** A schematic illustration for single-cell RNA sequencing (scRNA-seq) and analysis of samples from patients with HNSCC. **B,** t-SNE plotting for scRNA-seq results of fibroblasts and labeled according to the tumoral (brown) or adjacent normal (yellow) tissues origins. **C** and **D,** The proportion histograms of fibroblast cluster composition ratios in different samples and different fibroblast clusters in each sample. **E,** The expression of iCAF-associated, myCAF-associated and universal genes in the scRNA-seq results. Comparing genes presented in Figure 2D and 2E, these genes had limited discrepancy among cluster 5, 6 and 10. **F,** Density distribution of cells from individual fibroblast clusters along the first principal or second component of the principal component analysis (PCA). **G,** Pseudotime analysis of fibroblasts overlaid with the expression of ENG (CD105).

Supplementary Figure S3

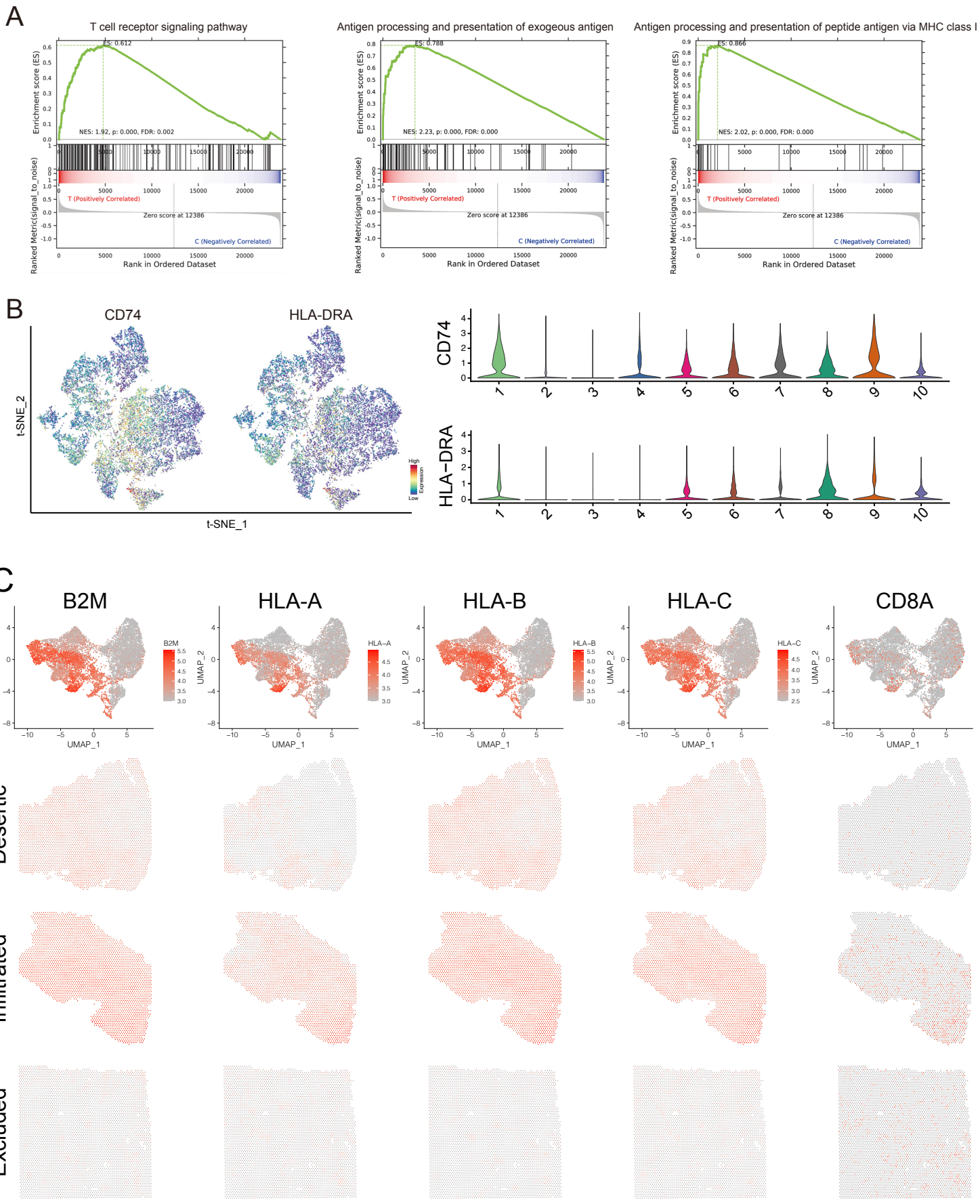

**Supplementary Figure S3.**

High expression levels of CXCLs and MHC class I molecules linked cluster 5 and CD8+ T cells. **A,** GSEA analysis of DGEs between fibroblasts from tumoral and adjacent normal tissues. **B,** HLA-DRA and CD74 expressions in the 10 clusters of fibroblasts. **C,** Spatial expression and distribution of MHC class I molecules in the three immune types of HNSCC.

Supplementary Figure S4

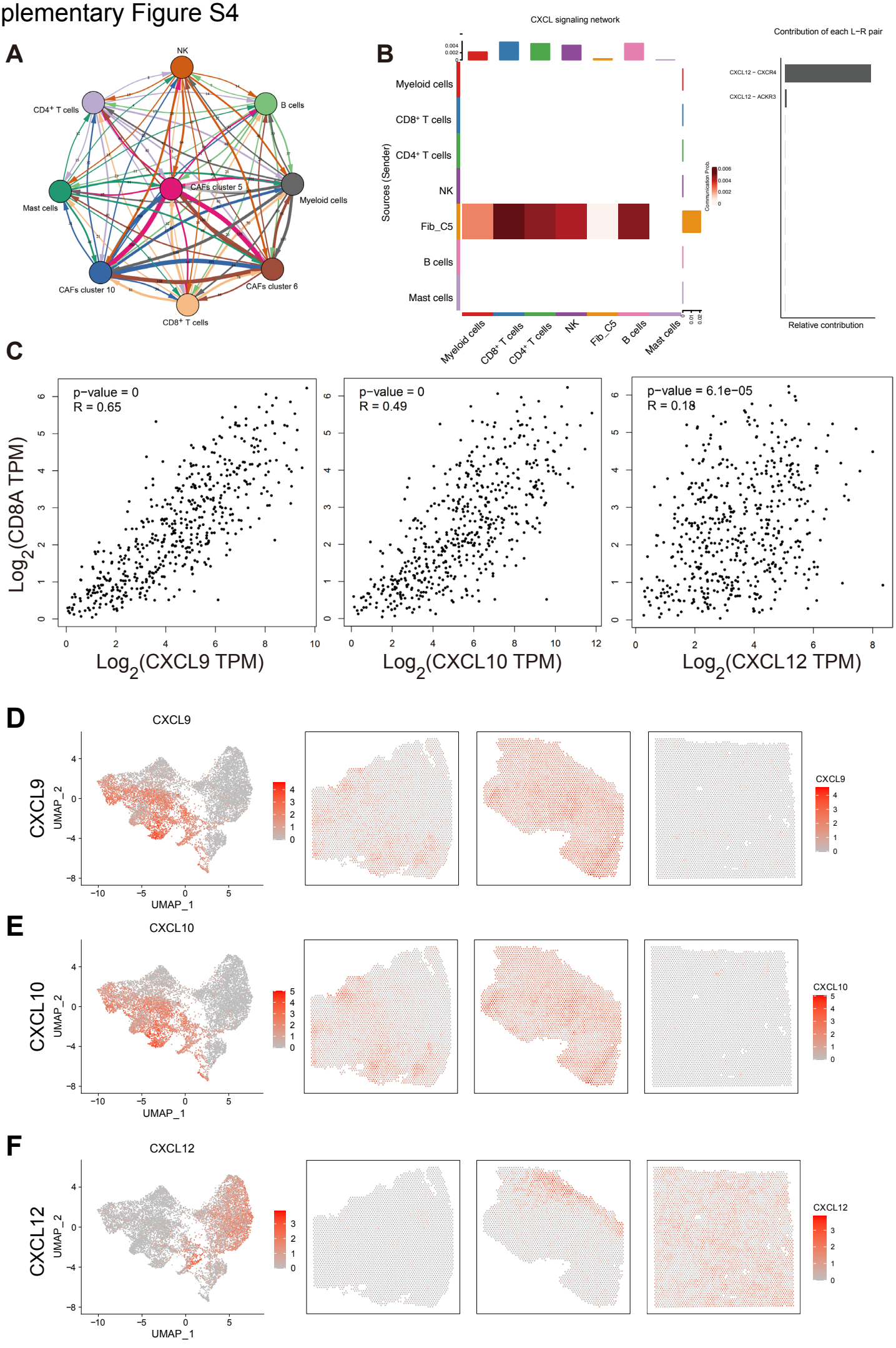

**Supplementary Figure S4.**

Spatial distribution of CXCLs and MHC class I molecules in different immune types of HNSCC. **A,** Cell Chat analysis between cluster 5 and cluster 6 fibroblasts and immune cells. **B,** CXCL signaling network among cluster 5 fibroblasts and immune cells. **C,** Correlation analysis of *CXCL9*/*10*/*12* and *CD8A* in HNSCC bulk-RNA sequencing results. **D-F**, Spatial expression and distribution of CXCLs, including (**D**) *CXCL9*, (**E**) *CXCL10* and (**F**) *CXCL12* in (left) desertic, (middle) infiltrated and (right) excluded immune types of HNSCC.

Supplementary Figure S5

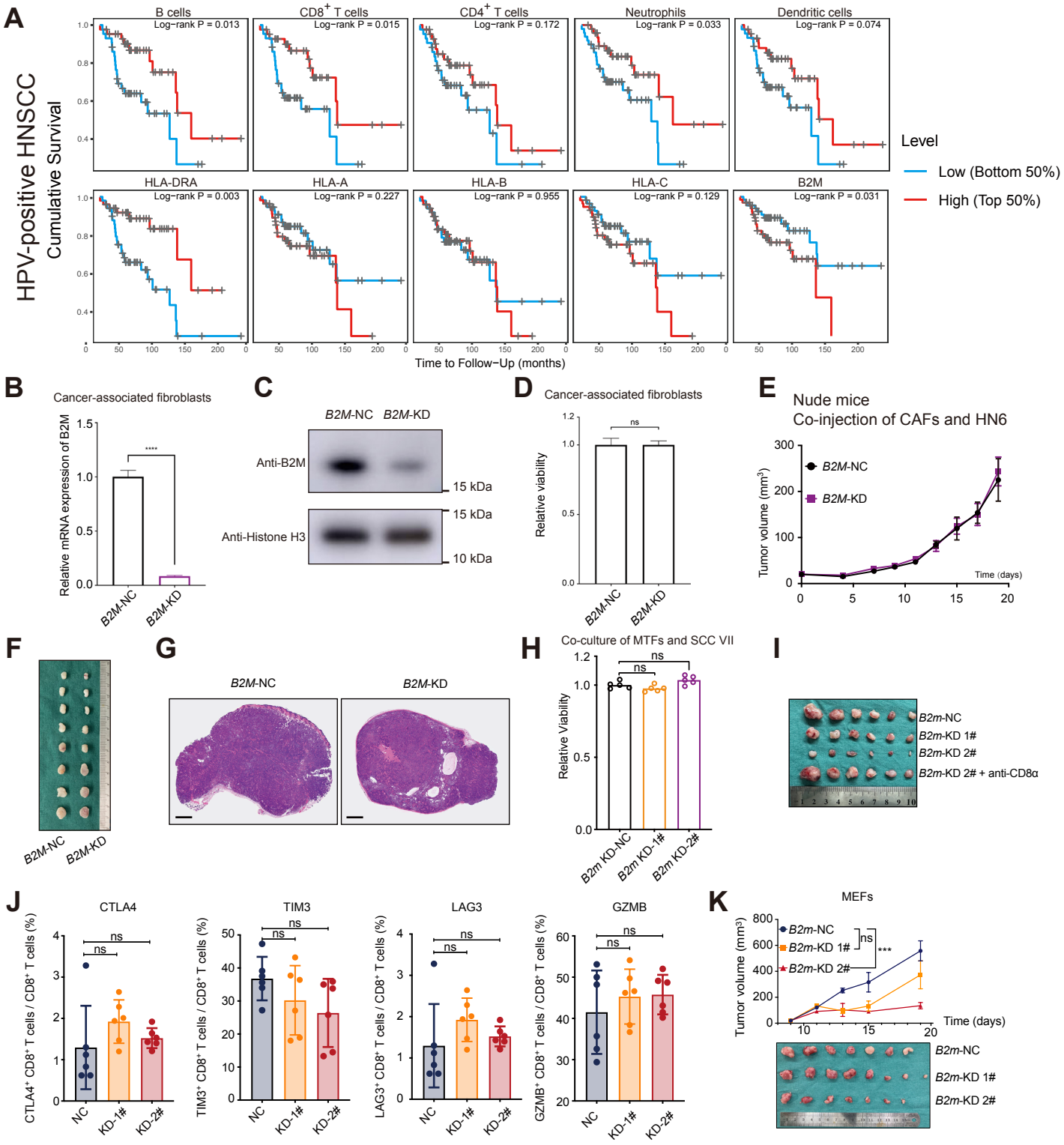

**Supplementary Figure S5.**

Correlation between MHC class I molecules in the fibroblasts and tumor progression. **A,** Kaplan–Meier survival plot comparing cumulative survival of HPV-positive HNSCC patients with different level of signatures for immune cells and selected genes. **B-G,** Subcutaneous co-injection of *B2M*-KD CAFs and HN6 in nude mice. **B** and **C,** The expression of *B2M* was knocked down in CAFs and (**D**) the viability examined by CCK-8 did not change. **E-G,** The subcutaneous tumor growth curve and their H&E images. Scale bar, 800 μm. **H,** The viability of SCC VII cells co-cultured with *B2m*-KD MTFs detected by CCK-8. **I,** The image for tumors isolated at day 19 after subcutaneous co-injection of SCCVII and MTFs in C3H/He mice. **J,** The proportion of $CD8^+$ T expressing cytotoxic cytokines (GZMB) and the immune checkpoints (CTLA4, TIM3, LAG3) in $CD8^+$ T cells isolated from subcutaneous tumors. **K,** The growth curve and the image for tumors derived from subcutaneous co-injection of SCCVII and MTFs.

# Supplementary Figure S6

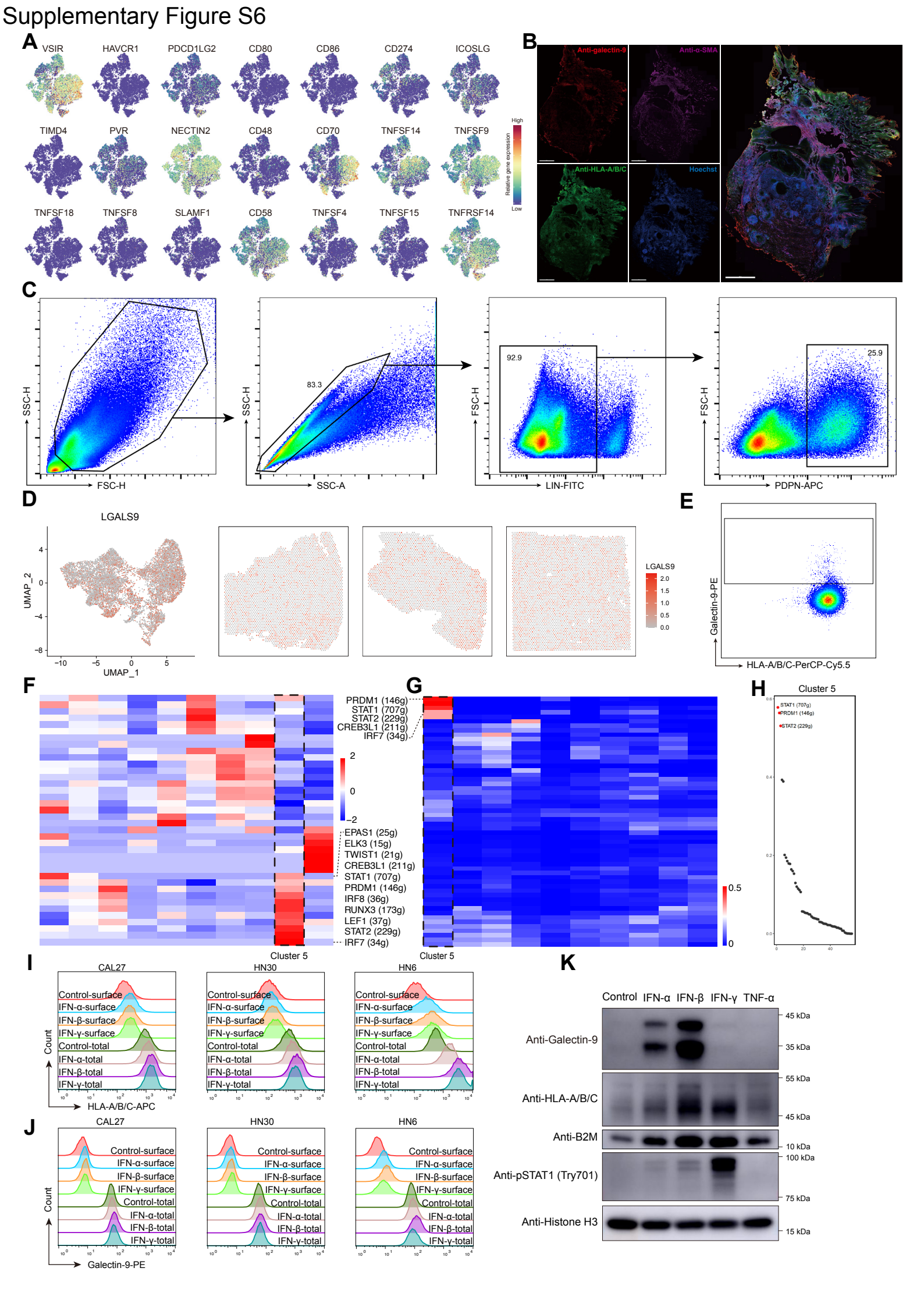

**Supplementary Figure S6.**

The expression and spatial distribution of galectin-9 in HNSCC. **A,** The expression of immune-checkpoint-related genes in fibroblasts. **B,** Representative large-scaled immunofluorescence results of human HNSCC tumor samples stained for nuclei (cyan), α-SMA (wine), galectin-9 (red), HLA-A/B/C (green). Scale bar, 2 mm. **C,** The flow cytometry gating strategy to isolate CAFs from HNSCC tumors for further analysis of galectin-9 and HLA-A/B/C. **D,** Spatial distribution of galectin-9 in different immune types of HNSCC. **E,** The expression of galectin-9 and HLA-A/B/C on CAFs cultured in vitro for two weeks. **F-H,** Scenic analysis for transcriptional regulons active in different clusters of CAFs indicated (**F**) activity levels of related regulons in each cluster and (**G**) specific regulons among these clusters. (**H**) The regulons in cluster 5 CAFs were ranked according to regulon specificity scores. **I** and **J,** The flow cytometry results for HLA-A/B/C and galectin-9 expression of HNSCC cell lines treated with IFNs. **K,** Western blotting results for HN6 cells treated with IFNs and TNF-α.

Supplementary Figure S7

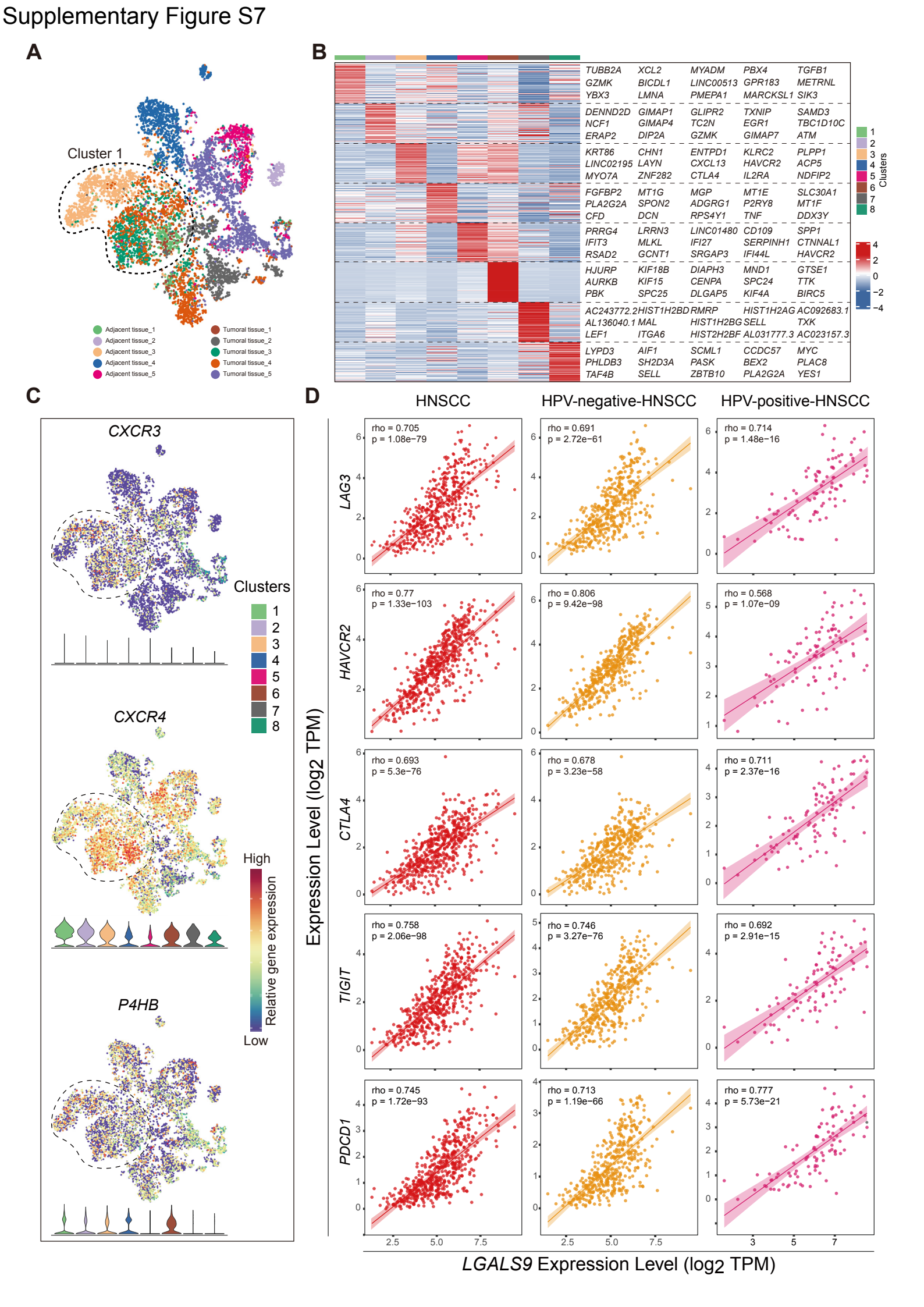

**Supplementary Figure S7.**

Clustering of $CD8^+$ T cells from single-cell RNA-sequencing of tumoral and adjacent HNSCC tissues. **A,** t-SNE plots of $CD8^+$ T cells overlaid with sample origins. **B,** Expression heatmap of marker genes of the 8 clusters of CD8+ T cells. **C,** t-SNE plots of CD8+ T cells colored by expression of genes (*CXCR3*, *CXCR4*, *P4HB*). **D,** Correlation between immune checkpoint molecules (*CTLA4*, *HAVCR2*, *LAG3*, *TIGIT*, *PDCD1*) and *LGALS9* (galectin-9) in bulk-RNA sequencing data from HNSCC, HPV-negative and HPV-positive HNSCC patients in TCGA database.

# Supplementary Figure S8

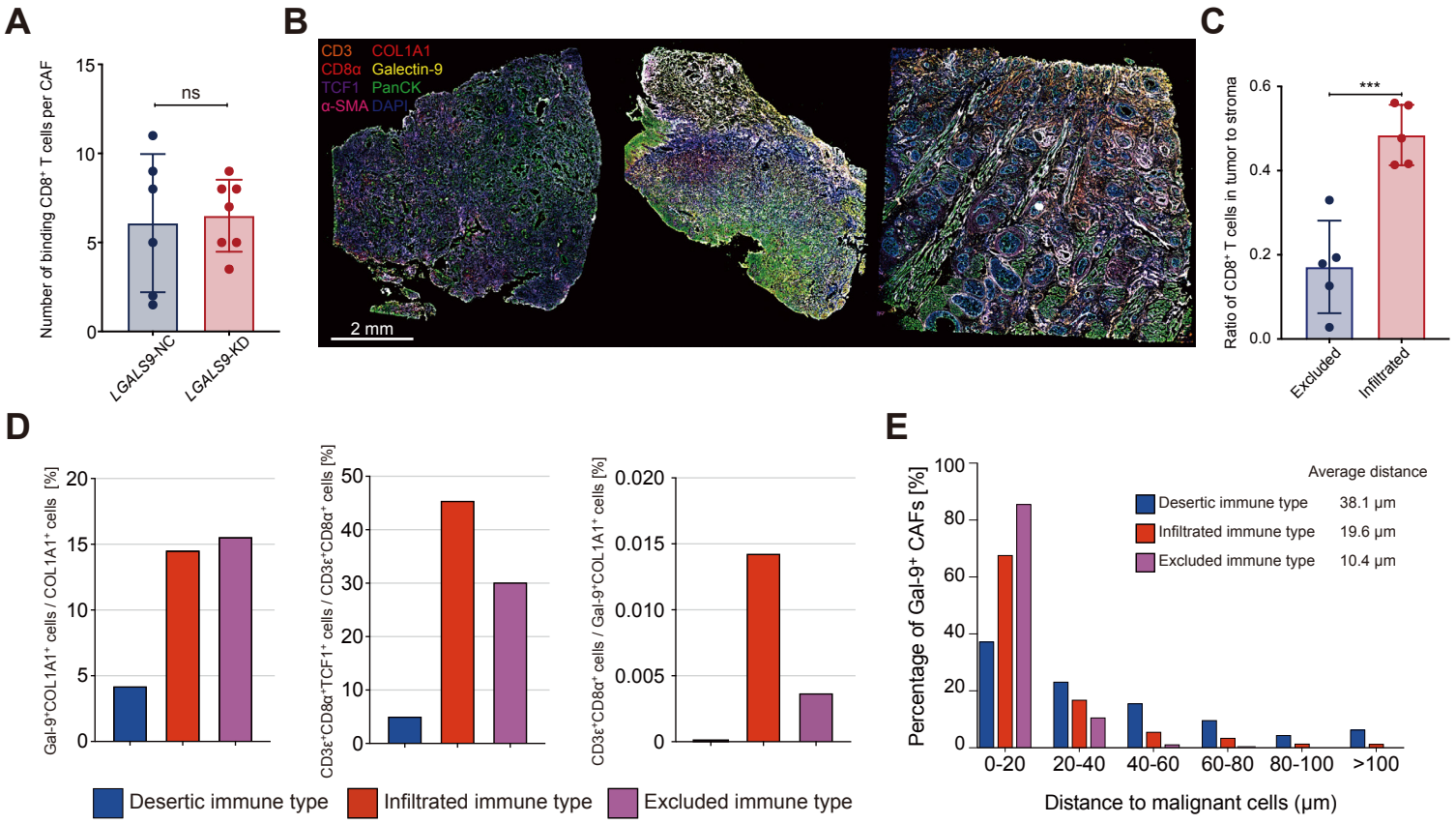

**Supplementary Figure S8.**

Galectin-9 is associated with dysfunctional differentiation of $TCF1^+CD8^+$ T cells. **A,** The number of CAF-binding $CD8^+$ T cells per CAF in the co-culture of these two types of cells after *LGALS9* KD in CAFs. **B,** Multiplex immunofluorescent staining (CD3, CD8α, PanCK, COL1A1, Gal-9, α-SMA) of three immune types HNSCC, the same specimens for spatial transcriptome sequencing. **C,** The ratio of the density of CD8+ T cells in tumor nests to that in stroma. **D,** Proportion of (left) $Gal\text{-}9^+$ fibroblasts in fibroblasts and (middle) $TCF1^+CD8^+$ T cells in $CD8^+$ T cells, and (right) the ratio of $CD8^+$ T cells compared with $Gal\text{-}9^+$ fibroblasts in the three immune types HNSCC. **E,** Proportion of $Gal\text{-}9^+$ CAFs ($Gal9^+COL1A1^+$ cells) in different ranges of distances between these cells to malignant cells ($PanCK^+$ cells). $Gal\text{-}9^+$ CAFs that have a distance equal to zero to malignant cells have been removed since COL1A1 and PanCK are extracellular proteins.